Calibration of Sampling Oscilloscopes With High-Speed Photodiodes

Tracy S. Clement, *Senior Member, IEEE*, Paul D. Hale, *Senior Member, IEEE*, Dylan F. Williams, *Fellow, IEEE*, C. M. Wang, Andrew Dienstfrey, and Darryl A. Keenan

***Abstract*—We calibrate the magnitude and phase response of equivalent-time sampling oscilloscopes to 110 GHz. We use a photodiode that has been calibrated with our electrooptic sampling system as a reference input pulse source to the sampling oscilloscope. We account for the impedance of the oscilloscope and the reference photodiode and correct for electrical reflections and distortions due to impedance mismatch. We also correct for time-base imperfections such as drift, time-base distortion, and jitter. We have performed a rigorous uncertainty analysis, which includes a Monte Carlo simulation of time-domain error sources combined with error sources from the deconvolution of the photodiode pulse, from the mismatch correction, and from the jitter correction.**

***Index Terms*—High-speed photodiode, impulse response, mismatch correction, oscilloscope calibration, sampling oscilloscope, uncertainty.**

I. Introduction

BROADBAND equivalent-time sampling oscilloscopes are routinely used to measure a variety of signals from data streams for communications to pulse time-of-flight measurements for biological applications. These instruments have the potential to be especially useful for the measurement of nonlinear microwave devices. In addition, techniques described here can be used to overcome the perceived problem of impedance mismatch in measuring microwave devices. At this time, there are several commercially available sampling oscilloscopes with bandwidths of 70–100 GHz. In the past, several methods have been described for measuring the impulse response or complex frequency response of broadband sampling oscilloscopes [1]–[16]. These methods fall into one of three categories, which are: 1) swept-sine calibrations; 2) "nose-to-nose" calibrations; and 3) calibration with a known pulse source. Our research extends previous techniques that use a known pulse source to higher frequencies and develops techniques for correcting significant sources of error including impedance mismatches and time-base distortions (TBDs). In addition, we provide a comprehensive uncertainty analysis for the complex frequency response of the oscilloscope.

The swept-sine calibration [3], [4] compares the amplitude of sine waves measured with the oscilloscope to the measurement of the power of the sine waves measured with a calibrated power meter. This comparison determines the magnitude response of the oscilloscope at each frequency. The swept-sine calibration is traceable to the calibration of the power meter and is the most accurate oscilloscope amplitude calibration currently available. The main disadvantage to the swept-sine calibration method is that it cannot determine the phase of the oscilloscope frequency response. Phase calibration of broadband oscilloscopes, however, is required for many microwave applications. In addition, without the phase information, it is impossible to determine the impulse response of the oscilloscope in the time domain.

Several groups have recently studied the nose-to-nose method as another possible oscilloscope calibration method [3]–[10]. The nose-to-nose technique uses as its pulse source a "kick-out" pulse that is generated by some oscilloscope sampler architectures. The nose-to-nose method relies on the assumption that this "kick-out" pulse is proportional to the impulse response of the oscilloscope. Several groups have studied the nose-to-nose assumption, and have quantified the error that this assumption introduces into the oscilloscope response determined from the nose-to-nose calibration [3], [4], [9], [10].

The concept of using a "known pulse source" to determine the response of the oscilloscope is relatively straightforward [11]. In an ideal system, the known pulse would be deconvolved from the measurement of the pulse source with the oscilloscope to determine the impulse response or complex frequency response of the oscilloscope. In practice, there can be many nonideal parts to the measurement of the known pulse source with the oscilloscope. In Section IV, we describe correction techniques for nonidealities such as drift, TBD, jitter, and impedance mismatch.

One of the main problems with the known pulse source technique is finding a pulse source that has a response sufficiently fast that enough energy exists at high frequencies to carry out the deconvolution. In the past, both electrical and opto-electronic methods have been used to generate pulses with very wide bandwidths [11]–[16]. Another problem with the known pulse technique is accurately determining the response of the pulse source. In the 1990s, the National Institute of Standards and Technology (NIST), Boulder, CO, used a superconducting oscilloscope with a bandwidth greater than 60 GHz as an "ideal" measurement system to determine the response of electrical pulse generators [11]. However, this approach is limited by both the bandwidth of the pulse generator and the imperfect response of the superconducting oscilloscope, which deviates from ideal at higher frequencies. Other groups have used an electrooptic sampling (EOS) method to determine the response of high-speed pulses that are generated in coplanar waveguide (CPW) [13]–[16]. The main limitation of this approach is in characterizing the transition from the CPW to the coaxial geometry of the oscilloscope and accounting for errors in that transition, and accounting for the frequency-dependent impedance of the oscilloscope. Our research improves upon these techniques.

Manuscript received December 15, 2005; revised March 25, 2006.

The authors are with the National Institute of Standards and Technology, Boulder, CO 80305 USA (e-mail: clementt@boulder.nist.gov).

Digital Object Identifier 10.1109/TMTT.2006.879135

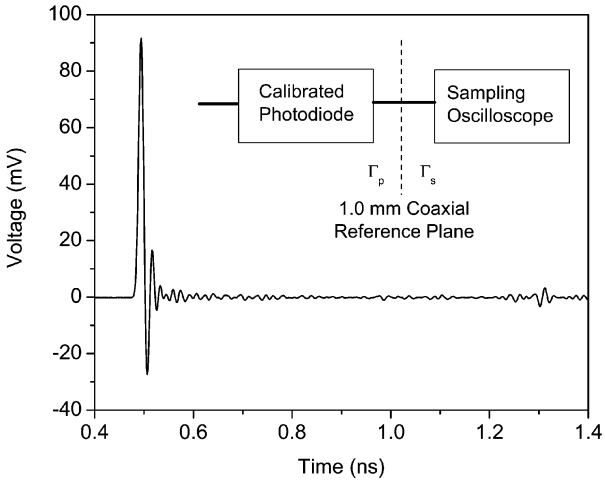

Fig. 1. Portion of the time-domain waveform generated by the photodiode and measured on the oscilloscope. The inset shows a schematic diagram of the waveform measurement setup.

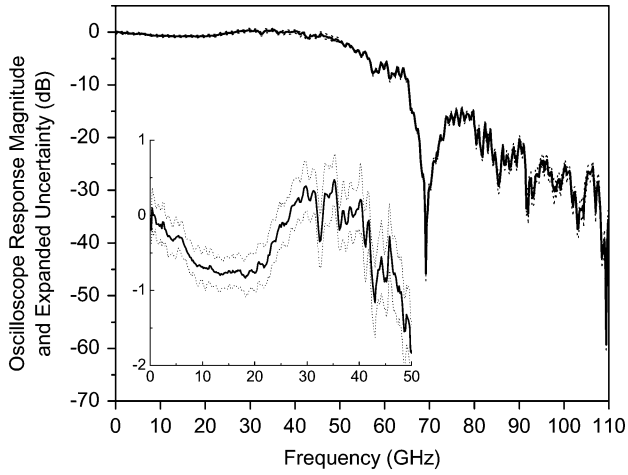

Fig. 2. Solid lines show the oscilloscope response magnitude (in decibels). The dashed lines indicate the 95% confidence interval for the calibrated response. The inset figure shows details of the response up to 50 GHz.

II. Experimental Waveform Measurements

Fig. 1 shows a portion of a typical time-domain waveform acquired for the calibration of the sampling oscilloscope. The inset of Fig. 1 shows a schematic diagram of the waveform measurement setup. Our known pulse source consists of a commercially available high-speed photodiode with bandwidth greater than 50 GHz (XPDV2020R, u2t Photonics AG, Berlin, Germany)[1] with a 1.85–1.0 mm coaxial adapter at the output. We calibrate the complex frequency response of the photodiode at the 1.0-mm coaxial plane from 0.2 to 110 GHz with our EOS system [17]–[19].

A mode-locked Er-doped fiber laser excites the calibrated photodiode with optical pulses that have a full-width at half-maximum (FWHM) pulsewidth of less than 70 fs at a center wavelength of 1550 nm, and a repetition rate of 8.66 MHz. This generates a train of ∼6-ps duration electrical pulses at the photodiode output. We use a reflective neutral-density filter to attenuate the laser output prior to coupling to the fiber pigtail of the photodiode. In order to avoid nonlinearities in both the photodiode and oscilloscope, we ensure that the peak voltage of the impulse as measured by the oscilloscope is less than 150 mV.

For the trigger signal, we use synchronous pulses from a pickoff in the Er-fiber laser. Another high-bandwidth photodiode converts the laser pulses into the electrical trigger signal.

In order to improve the signal-to-noise ratio for the oscilloscope measurements, we acquire 100 waveforms. Time-domain averaging of 100 waveforms can increase the signal-to-noise ratio of the magnitude response by 20 dB. As Fig. 2 shows, the magnitude response can fall by as much as 40 dB at 110 GHz, thus the benefit from averaging is significant. We do not average the waveforms prior to acquisition from the oscilloscope because any drift during the measurements can broaden the measured pulse in time. From the individual waveforms, we also obtain the noise statistics that we use for postprocessing algorithms that correct for drift and jitter.

The time base of the oscilloscopes we use is known to have distortion [5], [20], [21], including discontinuities every 4 ns. By adjusting the delay between the photodiode pulse and trigger pulse, we can move the position of the photodiode pulse relative to the time-base discontinuities. We take care to position the pulses so that the discontinuities will not occur during the main part of the pulse or where there is significant energy in the pulse or its reflections. We discuss the characterization and correction of this TBD in Section IV.

The waveform in Fig. 1 has a reflection that is caused by the impedance mismatch of the oscilloscope and photodiode at approximately 0.8 ns after the main pulse. Since we intentionally correct the measurements for the impedance mismatch of the source and oscilloscope (which can be manifest as reflections in the time domain), it is important to choose the time interval of the acquired waveform so that all of the significant energy due to reflections is captured. This is very different from many experiments where reflections are intentionally windowed out of the measured data, and where there is no accounting for impedance mismatch.

To ensure that we capture all of the reflections, we set the vertical scale on the oscilloscope to it lowest value, average the displayed waveforms on the oscilloscope, and pick an end point for the window where the averaged signal shows only noise. For the measurements with our photodiode, we typically use a 5-ns window. To ensure that this window captures all of the pulse information, we have compared the results taken with a window that is twice as large (10 ns), and see no significant differences in the response of the oscilloscope. The 5-ns interval setting also provides us with a convenient spacing of points in the frequency domain of 200 MHz.

It is also important to make sure that the spacing of points in the time domain is adequate for capturing the fast pulse events. When this is done, there is also no aliasing of energy in the frequency domain due to a sample rate that is too low. We sample 4096 points for each waveform, resulting in the spacing

[1]We use trade names only to specify our experimental conditions. This does not constitute an endorsement by NIST. Other products may perform as well or better.

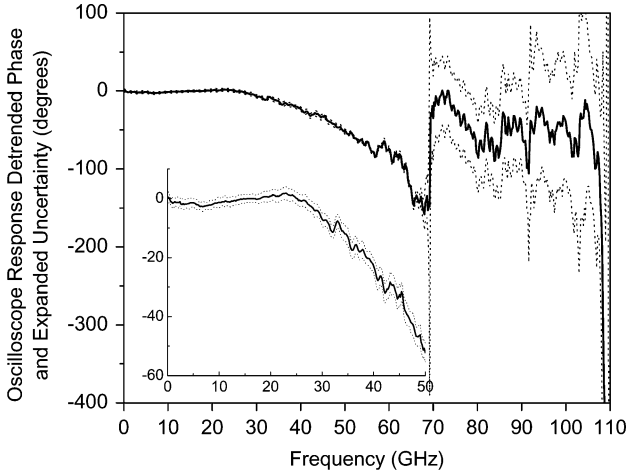

Fig. 3. Solid lines show the oscilloscope response phase in degrees. The dashed lines indicate the 95% confidence interval for the calibrated response. The inset figure shows details of the response up to 50 GHz.

of points in the time domain approximately equal to 1.22 ps (5 ns/4096). For our measured waveforms, the rise and fall times are ∼8–9 ps, thus we have more than six points within the rising or falling edges. This spacing of points in the time domain is equivalent to a Nyquist frequency of ∼400 GHz. For our system, the waveform information drops below the noise floor between 150–200 GHz, thus this sampling rate is sufficient. In addition, if we drop the number of points by half (to 2048), we see no significant changes in the measured oscilloscope response below 110 GHz.

III. Oscilloscope Response Results

In Section IV, we discuss in detail the corrections applied to the measured data. We correct for drift, TBD, jitter, impedance mismatch, and the known input pulse to obtain the complex frequency response at the 1.0-mm coaxial input of the oscilloscope. Figs. 2 and 3 show the complex frequency response results for a sampling oscilloscope that has a specified 3-dB bandwidth of greater than 50 GHz. The response is shown from 0.2 to 110 GHz on the larger plot. The smaller insets on each plot provide more detail of the response below 50 GHz. The dashed lines in both plots are calculated from the expanded uncertainty and indicate the 95% confidence interval of the results. Calculation of the uncertainty of the response is discussed in Section V.

In Fig. 2, the oscilloscope magnitude response is given in decibel units on the vertical axis. The response is normalized to the value at the lowest frequency point and is found to be independent of the input pulse amplitude for peak voltage less than 150 mV. The response falls by more than 40 dB at 110 GHz, and there is a very large notch in the response around 70 GHz. From the inset, we can see that the 3-dB bandwidth of this sampling oscilloscope is greater than 50 GHz. The standard uncertainty for this response is 0.2 dB at 50 GHz and 2.0 dB at 100 GHz.

Fig. 3 shows the phase response in degrees for the same sampling oscilloscope. For the phase response, we detrend the results by calculating a line with intercept equal to zero that best fits the phase data from 0.2 to 25 GHz in a least squares sense and subtracting that line. This detrending procedure corresponds to a pure shift in time. The jump in the phase around 70 GHz corresponds to the notch in the magnitude response at the same frequency. The standard uncertainty for this detrended phase response is 1.6° at 50 GHz. The phase uncertainty rises significantly with the phase jump around 70 GHz, and stays high at the higher frequencies. This increase in phase uncertainty happens because the magnitude is becoming very small at high frequencies, thus any uncertainty in the vector response as the magnitude of the vector approaches the origin leads to a much larger uncertainty in the phase.

The magnitude and phase response plotted in Figs. 2 and 3 were determined from multiple measurements of the same oscilloscope sampling head over more than two years time. The uncertainty includes the repeatability due to differences of many measurements made on the same day (within a set), and reproducibility due to differences between sets of data taken on different days, and with different experimental conditions.

IV. Corrections to Waveform Data

The waveform measured with the oscilloscope is two-dimensional (voltage versus time), and can have errors in either the time or voltage. A significant portion of the voltage errors are reduced by using the built-in dc calibration of the oscilloscope to correct for gain errors, offset errors, and "nonlinear distortion"—the manufacturer's term for the voltage distortion that can change at different voltage levels. The nonlinear distortion is corrected within the oscilloscope with an internal lookup table. Even with those errors reduced, the measured voltage waveform still has errors due to additive noise and quantization, and errors due to the finite response time of the oscilloscope. In general, for our measurements, we empirically find that the additive noise level is approximately 1-mV rms, while the quantization interval is approximately 50 μV. The quantization errors are small relative to the additive noise and are neglected for our results.

The oscilloscope time-base measurement errors include errors due to drift, TBD, and jitter. Below we describe the methods used for correcting each of these errors.

In addition to correcting for errors in the oscilloscope measurement of the waveforms, we also correct for the electrical mismatch between the photodiode pulse generator and oscilloscope, and we deconvolve the input electrical pulse. Fig. 4 shows a schematic flow diagram of the corrections that are applied to the measured data in order to obtain the frequency-domain impulse response for each sampling head.

A. Oscilloscope Time-Base Corrections

The first steps in our analysis are to correct the measured waveform data for errors due to the oscilloscope time base. We correct for drift, TBD, and jitter. In our correction procedures, we always correct for drift first, then TBD, and finally for jitter with the other frequency-domain magnitude corrections. Due to the nonlinear nature of the TBD errors, the order in the corrections can be important. To reduce the computation time, we first correct the individual waveforms for drift, then average and correct only the averaged waveform for the TBD. If, instead, we first correct for TBD of each individual waveform prior to correcting for drift and averaging, differences in the frequency-domain magnitude and phase responses are much smaller than the

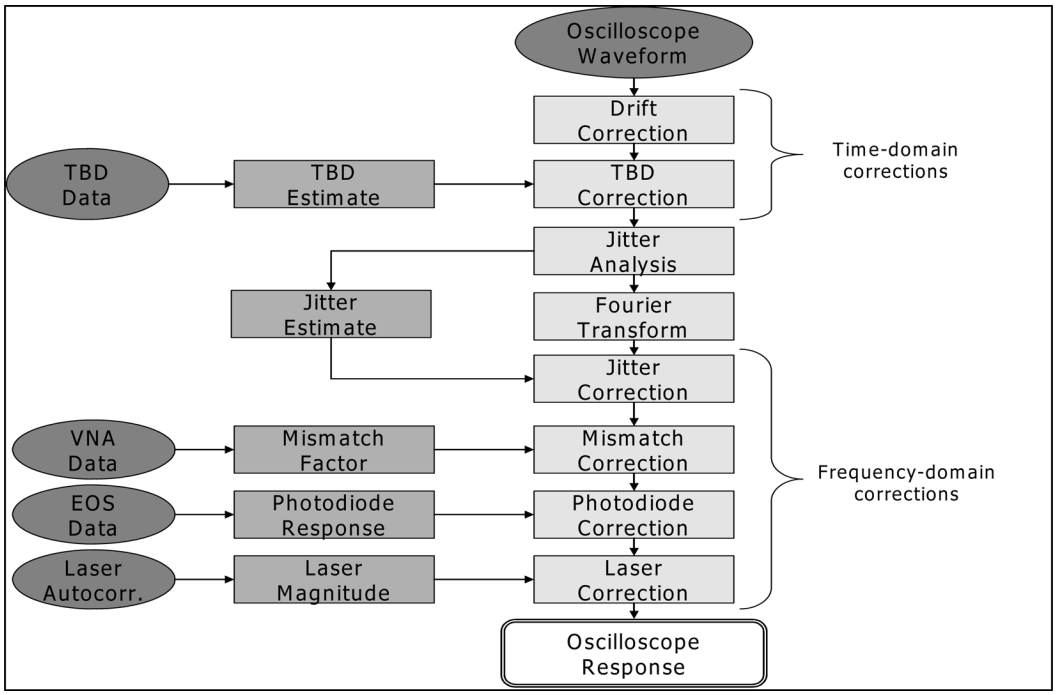

Fig. 4. Schematic flowchart of the corrections that are applied to the oscilloscope measurements to determine the oscilloscope response.

uncertainty in the response. Errors due to our order of processing the time-base errors is included in the uncertainty derived from the Monte Carlo analysis, which is described in Section V.

1) Drift: We define drift as a shift of the entire waveform in time. Since we acquire multiple waveforms, shifts in the waveforms in time will broaden the average of the pulses in time. One source of drift in sampling oscilloscope measurements is the temperature sensitivity of the trigger circuit [5]. Temperature stability in our laboratory during measurements is typically fairly good (± 1 °C), and we generally see very small drift in the measurements. This corresponds to a standard deviation of the drift of $\sim$0.3 ps, and a 0.19-dB attenuation at 110 GHz if we assume a Gaussian drift distribution.

To compensate for drift in the measurements, we align the individual waveforms before averaging, using an algorithm based on cross-correlation of all possible pairs of waveforms [22]. Each waveform is corrected for drift prior to averaging by Fourier transforming to the frequency domain, multiplying by $e^{i\omega\tau}$, where τ is the estimated drift for the waveform, and inverse Fourier transforming back to the time domain. The remaining corrections are performed on the drift-corrected average of the data.

2) TBD: TBD is a deterministic deviation in the sample times of the oscilloscope from the ideal evenly spaced sample times predicted by the oscilloscope [20]. We estimate the TBD for our measurement window by acquiring multiple sine waves with the oscilloscope and analyzing the sine-wave data with an efficient least squares fit algorithm [20], [21]. For the TBD estimate, we acquire four sets of sine-wave data, each with frequency equal to 9.25 or 10.25 GHz, and with a relative phase shift of 0° or 90° (in-phase and quadrature). To best capture the TBD under the same laboratory conditions as the oscilloscope waveform data, we determine the TBD of the oscilloscope for each set of experimental measurements.

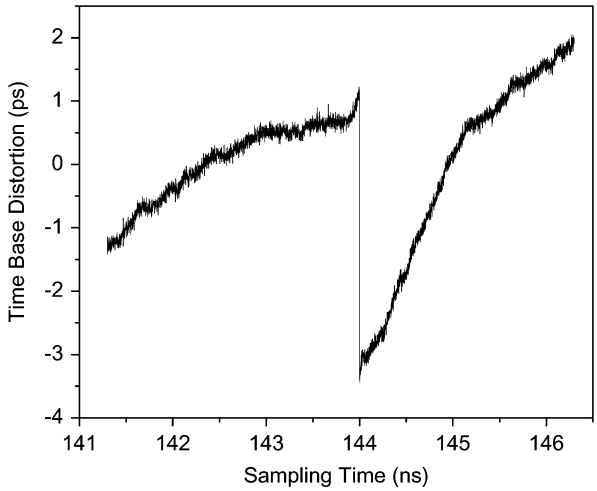

Fig. 5. TBD estimate for the sampling oscilloscope. The horizontal axis gives the sampling time expected from the oscilloscope, and the vertical axis gives the estimated error in that sampling time.

Fig. 5 shows a typical plot of the TBD for one of our oscilloscopes. In this figure, the horizontal axis represents the expected time at which the sample is taken (the number that the oscilloscope gives), and the vertical axis represents the difference between the expected sampling time and the actual sample time. The time axis of the averaged waveform is adjusted by the TBD estimate.

After correcting the sampling time of each point in the waveform, the resulting data, which is unevenly spaced in time, is interpolated onto an evenly spaced time grid using a regression

spline model [20], [23]. Finally, the averaged waveform is transformed to the frequency domain with a fast Fourier transform (FFT).

Some groups have suggested taking extra data points at both ends of the pulse waveform in order to provide enough data for a true interpolation at the ends for cases where the TBD results in time compression. For our measurements, the TBD typically does not result in time compression, and it is sufficient to use the same time window for the waveform data as for the TBD data. Furthermore, if there were time compression, our interpolation method produces reasonable results for our data because we measure time intervals that are long enough to ensure that the signal is below the noise level on both ends of the time window.

3) Jitter: In equivalent-time sampling, each sample is taken at a given delay after a trigger signal, meaning that each voltage–time pair in a waveform is taken with a new trigger. Due to this, jitter in the time-base circuitry and between the trigger signal and measured signal can have a large effect. We obtain a jitter estimate separately from each of the sets of measurements since it can be influenced by the specific sampler being measured, the specific trigger signal, and the trigger level.

We obtain the jitter estimate with a procedure that is based on the sample variance [24], [25]. Assuming that the jitter is small and has a symmetric probability density function, the variance of the measured signal due to jitter and additive noise can be expressed in a Taylor-series expansion as

$$\sigma_{\text{total}}^2 = \sigma_n^2 + \sigma_j^2 \left(\frac{dV}{dt}\right)^2 \tag{1}$$

where σ_{total}^2 is the total measured signal variance, σ_n^2 is the additive noise variance, σ_j^2 is the jitter variance, and dV/dt is the derivative of the time-domain waveform. To determine an initial estimate of the jitter variance, we use only the time samples for which the magnitude of the estimated derivative of the waveform exceeds a selected threshold. A parametric bootstrap approach is then used to eliminate the inherent bias in this method [25]. Typically, σ_j is less than 1 ps for these measurements, and the jitter is assumed to be normally distributed. We then correct the frequency-domain magnitude for the estimated jitter by multiplying by $\exp(\sigma_j^2\omega^2/2)$, where σ_j^2 is the estimated variance of the jitter. We note that the correction for jitter is an increasing function of frequency and can amplify noise at high frequencies, where the signal has rolled off to the noise floor.

B. Known Photodiode Input Pulse

The electrical waveform generated by the photodiode consists of the impulse response of the photodiode convolved with the laser pulse shape. Likewise, the measured data is a convolution of the waveform generated by the photodiode with the response of the oscilloscope sampling head. In the frequency domain, we correct the measured data to obtain the response of the sampling head by dividing the measured response by the complex frequency response of the photodiode and by the estimate of the laser excitation pulse.

1) Photodiode Response: The complex frequency response of the photodiode is determined with the NIST EOS system [17]–[19], [26]. The photodiode is calibrated at its 1.0-mm coaxial reference plane, and its response is determined from 0.2 to 110 GHz in 0.2-GHz steps. The known photodiode response is deconvolved by dividing it in the frequency domain from the complex frequency-domain oscilloscope data that have been corrected for the time-base errors. The photodiode response must have a significant signal level up to 110 GHz to obtain reasonable results from this division. The magnitude response of our high-speed photodiode falls off by only 12 dB at 110 GHz, providing a very good signal level for the deconvolution.

2) Laser Pulse: An estimate of the magnitude of the laser pulse envelope in the frequency domain is determined from a second-order autocorrelation measurement of the laser pulse. We fit the laser pulse magnitude (in decibels) up to 110 GHz with a fourth-order polynomial, and then correct the magnitude of the oscilloscope response with this quadratic function. Since the laser pulse is very short (less than 70-fs FWHM), corresponding to a very broad bandwidth in frequency (3-dB bandwidth $>$ 1 THz), the corrections to the oscilloscope response are very small (less than 0.019 dB at 110 GHz). One drawback to the use of the second-order autocorrelation is that all phase information about the laser pulse envelope is lost. However, following [27], we can conservatively estimate the maximum phase deviation due to asymmetry in the laser pulse envelope to be less than 0.0005° at 110 GHz. This is a negligible correction to the phase response of the oscilloscope.

C. Impedance Mismatch Correction

Electrical mismatch between the photodiode and oscilloscope can cause both multiple reflections of the pulse and dispersion of the time-domain signal. Electrical reflection coefficients for both the photodiode and oscilloscope are measured from 200 MHz to 110 GHz with a vector network analyzer. These measurements are limited to a maximum frequency of 110 GHz by the 1.0-mm coaxial connectors of the devices, and this provides the upper frequency limit for the overall oscilloscope calibration. The reflection coefficients for the photodiode and the oscilloscope are frequency dependent. Although they are designed to have a good 50-Ω match at low frequencies, the reflection coefficient is often as high as 0.5 at frequencies between 50–110 GHz. From the reflection-coefficient measurements, we correct for the mismatch by multiplying v_c, the frequency-domain data after applying all of the corrections described above, by the mismatch correction factor [28], resulting in v_s, the complex oscilloscope response

$$v_s = \frac{v_c}{(1 - \Gamma_p \Gamma_s)} \tag{2}$$

where Γ_p is the reflection coefficient of the photodiode and Γ_s is the reflection coefficient of the oscilloscope.

Fig. 6 shows the magnitude of the frequency-domain response of the oscilloscope both with (v_s), and without (v_c), the mismatch correction up to 60 GHz. The ripple on the uncorrected signal comes from the multiple reflections between the photodiode and oscilloscope, and must be corrected with (2) to determine the oscilloscope response. The importance of the TBD correction is especially apparent when combined with

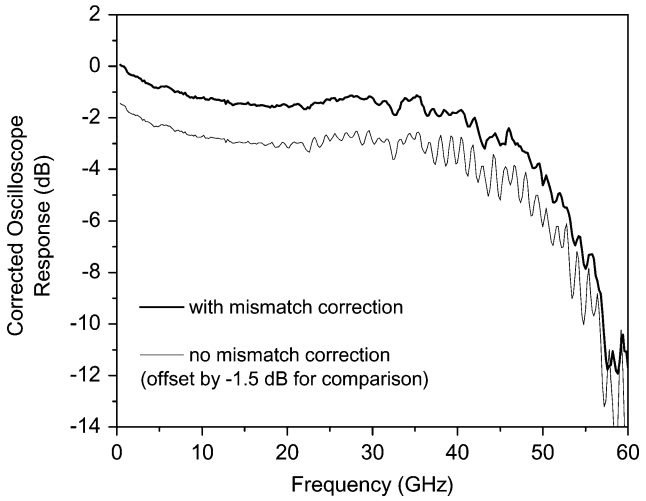

Fig. 6. Oscilloscope magnitude response without mismatch correction (grey line, offset by -1.5 dB for clarity) and with mismatch correction (black line).

the mismatch correction. Without TBD correction, the ripples due to electrical mismatch are only partially reduced because the spacing of the electrical reflections in the time domain is distorted by the TBD.

V. Uncertainty Analysis

A. Combining Uncertainties

We perform a point-by-point uncertainty analysis in the frequency domain [29]. Given a scalar random variable X with mean $E(X) = X_0$ and variance $\mathrm{var}(X) = \sigma^2[X]$, and variable $Y = F(X)$, where F is sufficiently differentiable, we have

$$E[Y] \approx F(X_0)$$
$$u^2[Y] \approx \left(\left. \frac{\partial F}{\partial x} \right|_{x=X_0} \right)^2 \sigma^2[X]. \tag{3}$$

The multivariate analog involving the Jacobian of F is straightforward; the details may be found in [29]. For most of the corrections described above, we use (3) to compute uncertainties. The main exception is for the determination of the uncertainty due to the time-base corrections described in Section IV. In this case, the functional forms are sufficiently complex that we instead use Monte Carlo analysis to determine the uncertainty of the frequency-domain results due to time-domain errors such as additive noise, correction of drift, and correction of TBD. The simulation includes both random variation in the observed time-domain waveform due to additive noise, jitter, and drift, and random variation in the TBD correction due to uncertainty in the TBD estimate. The results of this Monte Carlo simulation are time-domain waveforms, which are corrected for drift and TBD.

These simulated waveforms are individually transformed to the frequency domain, and the variance in the frequency domain is used to obtain the uncertainty due to the combined effects of additive noise, drift, TBD, and jitter uncertainties.

After the time-domain corrections, all of the remaining corrections (jitter, mismatch, photodiode response, laser pulse) are multiplicative in the frequency domain, implying that these corrections are additive when we look at the magnitude in decibels and are additive in the phase.

B. Components of Uncertainty

Table I summarizes the components of the total uncertainty and gives the typical standard uncertainty in magnitude and phase for each component at 50 and 100 GHz. The combined uncertainty is calculated from the sum of squared standard deviations of the uncertainties in the frequency domain. The expanded uncertainty can be obtained by multiplying by a coverage factor of 2 to estimate the 95% confidence interval about the mean estimated value [29].

1) Time-Domain Correction Uncertainties: We compute the variance due to the time-domain corrections from M (typically $M = 30$) simulation experiments. First, a reference waveform is calculated by correcting the measured waveforms for drift and TBD. For each of the M simulation experiments, we carry out a Monte Carlo analysis by constructing N (typically $N = 100$) time-domain waveform realizations by perturbing the reference waveform with a smoothed version of TBD, and with random variations due to drift, jitter, and additive noise. In addition, we construct one realization of the TBD by perturbing the smoothed version of the TBD with random variations due to noise in the TBD measurement. The parameters for the random perturbation are derived from the sample waveforms obtained from the oscilloscope. The jitter, drift, and additive noise variances used in the Monte Carlo simulation are estimated from the original data described in Section IV. For each simulation experiment, this results in N waveforms that are representative of the waveform data taken with the oscilloscope.

These N waveforms are then processed as if they were waveform data from the oscilloscope, correcting for drift and averaging, and estimating the jitter. We then correct this averaged simulation result for the perturbed TBD realization, and interpolate onto the evenly spaced grid.

We repeat this process for each of the M simulation experiments, resulting in M averaged waveforms (analogous to M laboratory experiments of N waveforms). We transform these M waveforms to the frequency domain and calculate the sample variances for both real and imaginary, or magnitude and phase, components due to the statistical deviations in the time-domain correction processes.

2) Mismatch Correction Uncertainty: The uncertainty in the mismatch correction is estimated from another Monte Carlo simulation that uses the uncertainties in the measurement of each scattering parameter. The simulation includes random variation in the reflection coefficients and scattering parameters due to uncertainty in the network analyzer measurements and the uncertainty in the coaxial standard definitions. For the reflection coefficients of the photodiode and oscilloscope, the network analyzer measurements are calibrated, and uncertainty in their calibration is determined using [30]. The standard uncertainty is determined from the manufacturer's specified worst case uncertainty (from [30]) for the standard definitions by dividing by a coverage factor of 3.

3) Uncertainty in Laser Pulse Shape: Since the correction for the laser pulse is very small, the uncertainty due to this cor-

TABLE I
TYPICAL VALUES FOR THE COMPONENTS OF UNCERTAINTY

Component	Magnitude Uncertainty (dB)		Phase Uncertainty (degrees)	
	50 GHz	100 GHz	50 GHz	100 GHz
Time-domain correction uncertainty	$<10^{-7}$	$<10^{-4}$	0.30	10.4
Mismatch correction uncertainty	0.02	0.07	0.12	0.46
Laser pulse width uncertainty	0.0017	0.007		
Photodiode response uncertainty	0.05	0.11	0.72	0.87
Repeatability	0.01	0.22	0.04	15

rection is also very small compared to all the other uncertainties. We conservatively estimate the uncertainty due to the laser pulse correction in magnitude as being equal to the half of the magnitude correction, giving an uncertainty of only 0.010 dB at 110 GHz. For the extremely small phase correction, the error is negligible compared to the other uncertainties and is neglected in the total phase uncertainty.

4) Photodiode Response Uncertainty: The uncertainty in the photodiode response is estimated from measurements of the response with the NIST EOS system. Systematic uncertainty in the EOS measurement of the photodiode response includes uncertainty in the mismatch correction due to uncertainties in the measurement of on-wafer scattering parameters, uncertainty in the measurement of coaxial scattering parameters, and uncertainty due to the finite impulse response of the EOS system [17], [18]. We do not include uncertainty due to the finite measurement time window in the EOS system or possible piezoelectric resonances. These effects may increase the uncertainty at the lowest frequencies, but are negligible at higher frequencies.

5) Repeatability: To estimate the statistically derived type-A uncertainty [29] in our measurements due to repeatability, we typically perform five sets of repeat measurements. The complex frequency response is obtained from each set of measurements as described above. Standard uncertainty in the mean of the magnitude and phase is obtained from the standard deviation of the five resulting responses.

VI. DISCUSSION

In order to check the oscilloscope complex frequency response results, we performed a swept-sine calibration of the magnitude of the complex frequency-domain response [31]. The top plot of Fig. 7 shows the magnitude response obtained from the known photodiode-based calibration described here (dark line) along with the response obtained from a swept-sine calibration (lighter line). The two responses agree very well over the region where we have swept-sine data (up to 40 GHz). The bottom plot in Fig 7 shows the difference in decibel units between the two calibrations. The difference is less than ± 0.3 dB from 0.2 to 40 GHz, and the difference is significantly less than the combined uncertainties of both measurements.

The 0.2-GHz spacing of points in the oscilloscope calibration is limited by the data acquisition in the calibration of the photodiode and not by inherent limitations in the oscilloscope measurements. However, due to this limit, we are unable to capture ripples or features with a period of less than 0.2 GHz. We have calibrated the magnitude response with the swept-sine technique for various spacing of frequency points and find no significant lower frequency features of the oscilloscope response [31].

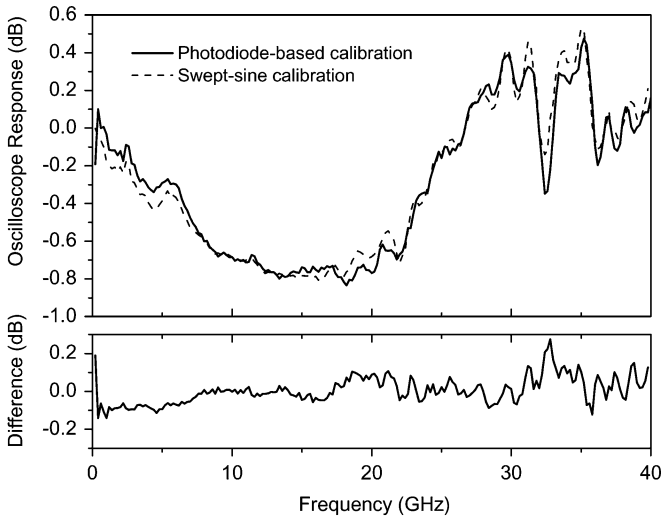

Fig. 7. Comparison of photodiode-based known pulse calibration described here with a swept-sine calibration of the oscilloscope. The magnitude of the oscilloscope response is plotted in the top graph, and the difference between the two methods is plotted in the bottom graph.

The calibration of the photodiode with our EOS system has limited resolution at low frequencies due to the finite measurement window of the sampling system. This results in poor estimates of the response of the oscilloscope at low frequencies. Knowing the low-frequency response of the oscilloscopes can become very important, especially in determining the step response in the time domain [13]. It is possible to get a very good estimate of the magnitude of the frequency response at low frequencies with the swept-sine technique described in Section I. We are currently investigating ways to combine the magnitude response at low frequencies obtained from the swept-sine technique with the magnitude and phase response at higher frequencies obtained from the techniques presented here in order to obtain a more complete estimate of the complex frequency response, which can then be used to calculate the impulse or step response in the time domain [31].

VII. CONCLUSION

We have calibrated the complex frequency response of high-speed oscilloscopes to 110 GHz using a calibrated photodiode as a reference pulse source. The results include corrections for impedance mismatch, drift, jitter, TBD, and the photodiode impulse. We have presented a complete uncertainty analysis for the complex frequency response calibration. We have verified

the calibration by comparison with a swept-sine calibration of the oscilloscope.

With our calibrated oscilloscope, we can now determine the response of a variety of sources (pulse sources, step inputs, communication signals, and circuits including harmonics and other distortion products generated by nonlinearities). We can deconvolve the response of the oscilloscope from the measurement of high-speed signals and improve the calibration of pulse sources.

Appendix I
Calibration With a Coaxial Adapter Between the Photodiode and Oscilloscope

In order to calibrate the oscilloscope at a different coaxial reference plane (e.g., at the 2.4-mm coaxial connector on the front of the sampling head instead of at the 1.0-mm coaxial connector of the adapter), it is necessary to extend our mismatch correction to include the adapter's s-parameters. If we place an adapter with scattering parameters S_{ij} between the generator and oscilloscope, the equation for the oscilloscope response becomes

$$h = v_s v_g \times \left(\frac{1 - \Gamma_p S_{11} - \Gamma_s S_{22} - \Gamma_p \Gamma_s (S_{21} S_{12} - S_{11} S_{22})}{S_{21}} \right). \tag{4}$$

This allows calibration through adapters and to different waveguide types and sizes.

Acknowledgment

The authors thank K. Coakley, National Institute of Standards and Technology (NIST), Boulder, CO, for his work in the development of the Monte Carlo simulations and H. Reader, University of Stellenbosch, Stellenbosch, South Africa, for his helpful comments on this paper's manuscript.

References

[1] K. A. Remley and D. F. Williams, "Sampling oscilloscope models and calibrations," in *IEEE MTT-S Int. Microw. Symp. Dig.*, 2003, pp. 1507–1510.

[2] M. Kahrs, "50 years of RF and microwave sampling," *IEEE Trans. Microw. Theory Tech.*, vol. 51, no. 6, pp. 1787–1805, Jun. 2003.

[3] P. D. Hale, T. S. Clement, K. J. Coakley, C. M. Wang, D. C. DeGroot, and A. P. Verdoni, "Estimating magnitude and phase response of a 50 GHz sampling oscilloscope using the 'nose-to-nose' method," in *ARFTG Conf. Dig.*, Jun. 2000, vol. 55, pp. 335–342.

[4] D. C. DeGroot, P. D. Hale, M. V. Bossche, F. Verbeyst, and J. Verspecht, "Analysis of interconnection networks and mismatch in the nose-to-nose calibration," in *ARFTG Conf. Dig.*, Jun. 2000, vol. 55, pp. 116–121.

[5] J. Verspecht and K. Rush, "Individual characterization of broadband sampling oscilloscopes with a nose-to-nose calibration procedure," *IEEE Trans. Instrum. Meas.*, vol. 43, no. 2, pp. 347–354, Apr. 1994.

[6] K. Rush, S. Draving, and J. Kerley, "Characterizing high-speed oscilloscopes," *IEEE Spectr.*, vol. 27, no. 9, pp. 38–39, Sep. 1990.

[7] J. Verspecht, "Broadband sampling oscilloscope characterization with the 'nose-to-nose' calibration procedure: A theoretical and practical analysis," *IEEE Trans. Instrum. Meas*, vol. 44, no. 6, pp. 991–997, Dec. 1995.

[8] N. G. Paulter and D. R. Larson, "An examination of the spectra of the 'kick-out' pulses for a proposed sampling oscilloscope calibration method," *IEEE Trans. Instrum. Meas*, vol. 50, no. 5, pp. 1221–1223, Oct. 2001.

[9] K. A. Remley, "The impact of internal sampling circuitry on the phase error of the nose-to-nose oscilloscope calibration," NIST, Boulder, CO, Tech. Note 1528, Aug. 2003.

[10] ——, "Nose-to-nose oscilloscope calibration phase error inherent in the sampling circuitry," in *ARFTG Conf. Dig.*, Dec. 2002, vol. 60, pp. 85–97.

[11] W. L. Gans, "Dynamic calibration of waveform recorders and oscilloscopes using pulse standards," *IEEE Trans. Instrum. Meas*, vol. 39, no. 6, pp. 952–957, Dec. 1990.

[12] J. P. Deyst, N. G. Paulter, T. M. Souders, G. N. Stenbakken, and T. A. Daboczi, "Fast pulse oscilloscope calibration system," *IEEE Trans. Instrum. Meas.*, vol. 47, no. 5, pp. 1037–1041, Oct. 1998.

[13] D. Henderson and A. G. Roddie, "Calibration of fast sampling oscilloscopes," *Meas. Sci. Technol.*, no. 1, pp. 673–679, 1990.

[14] A. J. A. Smith, A. G. Roddie, and P. D. Woolliams, "Optoelectronic techniques for improved high speed electrical risetime," in *IEEE MTT-S Int. Microw. Symp. Dig.*, Jun. 2002, vol. 3, pp. 1501–1504.

[15] D. Henderson, A. G. Roddie, and A. J. A. Smith, "Recent developments in the calibration of fast sampling oscilloscopes," *Proc. Inst. Elect. Eng.—Sci., Meas. Technol.*, vol. 139, no. 5, pp. 254–260, Sep. 1992.

[16] S. Seitz, M. Bieler, M. Spitzer, K. Pierz, G. Hein, and U. Siegner, "Optoelectonic measurement of the transfer function and time response of a 70 GHz sampling oscilloscope," *Meas. Sci. Tech.*, vol. 16, no. 10, pp. L7–L9, Oct. 2005.

[17] D. F. Williams, P. D. Hale, T. S. Clement, and J. M. Morgan, "Calibrating electro-optic sampling systems," in *IEEE MTT-S Int. Microw. Symp. Dig.*, May 2001, vol. 3, pp. 1527–1530.

[18] D. F. Williams, P. D. Hale, T. S. Clement, and C. M. Wang, "Uncertainty of the NIST electrooptic sampling system," NIST, Boulder, CO, Tech. Note 1535, Dec. 2004.

[19] D. F. Williams, P. D. Hale, T. S. Clement, and J. M. Morgan, "Mismatch corrections for electro-optic sampling systems," in *ARFTG Conf. Dig.*, Nov. 2000, vol. 56, pp. 141–145.

[20] C. M. Wang, P. D. Hale, and K. J. Coakley, "Least-squares estimation of time-base distortion of sampling oscilloscopes," *IEEE Trans. Instrum. Meas*, vol. 48, no. 6, pp. 1324–1332, Dec. 1999.

[21] C. M. Wang, P. D. Hale, K. J. Coakley, and T. S. Clement, "Uncertainty of oscilloscope timebase distortion estimate," *IEEE Trans. Instrum. Meas*, vol. 51, no. 1, pp. 53–58, Feb. 2002.

[22] K. J. Coakley and P. D. Hale, "Alignment of noisy signals," *IEEE Trans. Instrum. Meas*, vol. 50, no. 1, pp. 141–149, Feb. 2001.

[23] Y. Rolain, J. Schoukens, and G. Vandersteen, "Signal reconstruction for non-equidistant finite length sample sets: A 'KIS' approach," *IEEE Trans. Instrum. Meas.*, vol. 47, no. 5, pp. 1046–1052, Oct. 1998.

[24] J. Verspecht, "Compensation of timing jitter-induced distortion of sampled waveforms," *IEEE Trans. Instrum. Meas*, vol. 43, no. 5, pp. 726–732, Oct. 1994.

[25] K. J. Coakley, C. M. Wang, P. D. Hale, and T. S. Clement, "Adaptive characterization of jitter noise in sampled high-speed signals," *IEEE Trans. Instrum. Meas*, vol. 52, no. 5, pp. 1537–1547, Oct. 2003.

[26] T. S. Clement, P. D. Hale, D. F. Williams, and J. M. Morgan, "Calibrating photoreceiver response to 110 GHz," in *15th Annu. IEEE Lasers Electro-Optics Soc. Conf. Dig.*, Glasgow, U.K., Nov. 10–14, 2002, pp. 877–878.

[27] J. Verspecht, "Quantifying the maximum phase-distortion error introduced by signal samplers," *IEEE Trans. Instrum. Meas*, vol. 46, no. 3, pp. 660–666, Jun. 1997.

[28] D. F. Williams, A. Lewandowski, T. S. Clement, C. M. Wang, P. D. Hale, J. M. Morgan, D. Keenan, and A. Dienstfrey, "Covariance based uncertainty analysis of the NIST electrooptic sampling system," *IEEE Trans. Microw. Theory Tech.*, vol. 54, no. 1, pp. 481–491, Jan. 2006.

[29] BIPM, IEC, IFCC, ISO, IUPAP, and OIML, "Guide to the expression of uncertainty in measurement," *Int. Org. Standard.*, pp. 1–101, 1993.

[30] HP8510 Specifications and Performance Verification Analysis Software. Hewlett-Packard, Palo Alto, CA, part 08510-10033, program revision A.05.00, data revision A.05.00.

[31] A. Dienstfrey, P. D. Hale, D. A. Keenan, T. S. Clement, and D. F. Williams, "Minimum-phase calibration of sampling oscilloscopes," *IEEE Trans. Microw. Theory Tech.*, vol. 54, no. 8, pp. 3197–3208, Aug. 2006.

Tracy S. Clement (S'89–M'92–SM'05) received the Ph.D. degree in electrical engineering from Rice University, Houston, TX, in 1993. Her Ph.D. research concerned the development and study of novel ultrashort pulse and very short wavelength lasers.

Since 1998, she has been with the Optoelectronics Division, National Institute of Standards and Technology (NIST), Boulder, CO. Her current research interests include the development of measurement systems for high-speed electrooptic components, as well as ultrashort pulse laser measurements. Prior to joining the Optoelectronics Division, she was an Associate Fellow with JILA, in the Quantum Physics Division, NIST, and was an Assistant Professor Adjoint with the Department of Physics, University of Colorado at Boulder. From 1993 to 1995, she was a Director's Post-Doctoral Fellow with the Los Alamos National Laboratory, Los Alamos, NM.

Dr. Clement was the recipient of the Department of Commerce Silver Medal.

Paul D. Hale (M'01–SM'01) received the Ph.D. degree in applied physics from the Colorado School of Mines, Golden, CO, in 1989.

Since 1989, he has been with the Optoelectronics Division, National Institute of Standards and Technology (NIST), Boulder, CO, where has conducted research in birefringent devices, mode-locked fiber lasers, fiber chromatic dispersion, broadband lasers, interferometry, polarization standards, and high-speed opto-electronic measurements. He is currently Leader of the High-Speed Measurements Project in the Sources and Detectors Group. His research interests include high-speed opto-electronic and microwave measurements and their calibration.

Dr. Hale is currently an associate editor for the JOURNAL OF LIGHTWAVE TECHNOLOGY. He was the recipient of the Department of Commerce Bronze, Silver, and Gold Awards, two Automatic RF Techniques Group (ARFTG) Best Paper Awards, and the NIST Electrical Engineering Laboratory's Outstanding Paper Award.

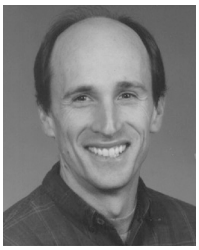

Dylan F. Williams (M'80–SM'90–F'02) received the Ph.D. degree in electrical engineering from the University of California at Berkeley, in 1986.

In 1989, he joined the Electromagnetic Fields Division, National Institute of Standards and Technology (NIST), Boulder, CO, where he develops metrology for the characterization of monolithic microwave integrated circuits and electronic interconnects. He has authored or coauthored over 80 technical papers.

Dr. Williams is currently Editor-in-Chief of the IEEE TRANSACTIONS ON MICROWAVE THEORY AND TECHNIQUES. He was the recipient of the Department of Commerce Bronze and Silver Medals, two Electrical Engineering Laboratory's Outstanding Paper Awards, two Automatic RF Techniques Group (ARFTG) Best Paper Awards, the ARFTG Automated Measurements Technology Award, and the IEEE Morris E. Leeds Award.

C. M. Wang received the Ph.D. degree in statistics from Colorado State University, Fort Collins, in 1978.

He is currently a Mathematical Statistician with the Statistical Engineering Division, National Institute of Standards and Technology (NIST), Boulder, CO. His research interests include statistical metrology and the application of statistical methods to physical sciences.

Dr. Wang is a Fellow of the American Statistical Association. He was the recipient of the Department of Commerce Bronze Medal.

Andrew Dienstfrey received the B.A. degree in mathematics from Harvard University, Cambridge, MA, in 1990, and the Ph.D. degree in mathematics from the Courant Institute of Mathematical Sciences, New York, NY, in 1998.

From 1998 to 2000, he was a Post-Doctoral Scientist with the Courant Institute, where he investigated methods for remote sensing of dielectric properties of superconducting thin films. In 2000, he joined the Mathematical and Computational Sciences Division, National Institute of Standards and Technology (NIST), Boulder, CO. His research interests include theoretical and computational aspects of periodic scattering problems in acoustics and electromagnetics.

Darryl A. Keenan received the B.S. degree in physics from the University of Colorado at Boulder, in 1996.

In 1989, he joined the National Institute of Standards and Technology (NIST) [then the National Bureau of Standards (NBS)], Boulder, CO, and has since been a member of the Sources and Detectors Group, Optoelectronics Division. He has run optical laser metrology laboratories including low-power continuous wave (CW) from the visible to near infrared, high-power CW at far infrared, Q-switched Nd : YAG at near infrared, and Excimer at ultraviolet to deep ultraviolet. He has worked with colleagues to develop optical fiber connector characterization and to develop a system for measuring detector nonlinearity at 193 nm. His current areas of research include optical laser metrology at 193 and 248 nm and time- and frequency-domain characterization of oscilloscopes using swept sine measurements and calibrated photodiodes.